HHS Public Access

Author manuscript

Nat Chem Biol. Author manuscript; available in PMC 2016 March 01.

Published in final edited form as:

Nat Chem Biol. 2015 September ; 11(9): 678–684. doi:10.1038/nchembio.1863.

A new metal binding domain involved in cadmium, cobalt and zinc transport

Aaron T. Smith[1], **Dulmini Barupala**[2], **Timothy L. Stemmler**[2], and **Amy C. Rosenzweig**[1,*]

[1]Departments of Molecular Biosciences and of Chemistry, Northwestern University, Evanston, Illinois, USA

[2]Department of Pharmaceutical Sciences and Cardiovascular Research Institute, Wayne State University, School of Medicine, Detroit, Michigan, USA

Abstract

The P_{1B}-ATPases, which couple cation transport across membranes to ATP hydrolysis, are central to metal homeostasis in all organisms. An important feature of P_{1B}-ATPases is the presence of soluble metal binding domains that regulate transport activity. Only one type of MBD has been characterized extensively, but bioinformatics analyses indicate that a diversity of MBDs may exist in nature. Here we report the biochemical, structural, and functional characterization of a new MBD from the *Cupriavidus metallidurans* P_{1B-4}-ATPase CzcP (CzcP MBD). The CzcP MBD binds two Cd^{2+}, Co^{2+}, or Zn^{2+} ions in distinct and unique sites, and adopts an unexpected fold consisting of two fused ferredoxin-like domains. Both in vitro and in vivo activity assays using full length CzcP, truncated CzcP, and several variants indicate a regulatory role for the MBD and distinct functions for the two metal binding sites. Taken together, these findings elucidate a previously unknown MBD and suggest new regulatory mechanisms for metal transport by P_{1B}-ATPases.

INTRODUCTION

The P_{1B}-ATPases are central to metal homeostasis in all kingdoms of life. These transporters, members of the larger P-type ATPase superfamily[1], couple ATP hydrolysis to the translocation of metal ions across membranes. Combined biochemical and genomic data indicate that P_{1B}-ATPases are involved in the transport of Mn^{2+}, Co^{2+}, $Cu^{+/2+}$, Zn^{2+}, Cd^{2+}, Hg^{2+}, and Pb^{2+}, and may also play a role in Fe^{2+} and Ni^{2+} transport[2-4]. In prokaryotes, P_{1B}-ATPases function in metalloprotein biosynthesis and detoxification of cytoplasmic metal

*To whom correspondence should be addressed. amyr@northwestern.edu.

Author contributions

A. T. S. and D. B. conducted all experiments, and A. C. R. and T. L. S. directed the research. A. T. S., D. B., T. L. S., and A. C. R. wrote the manuscript.

Competing financial interests

The authors declare no competing financial interests.

Additional information

Supplementary information is available in the online version of this paper.

ions via efflux. In addition, some bacterial P_{1B}-ATPases are necessary for infection[5,6], and thus represent a potential new frontier for antibiotic development. Eukaryotic P_{1B}-ATPases are critically important in metalloprotein assembly and metal distribution[7,8]. In humans, mutations in the Cu^+-transporting P_{1B}-ATPases ATP7A and ATP7B lead to Menkes syndrome and Wilson disease, respectively[9]. Given the broad importance of P_{1B}-ATPases, it is surprising how little is known about their function. Although several crystal structures are available[10-12], the details of metal binding, the molecular basis for metal ion specificity, and the mechanism of metal transport remain unclear.

The archetypal P_{1B}-ATPase is composed of six core transmembrane helices (TMs), a soluble actuator domain (AD) between TM2 and TM3, and a soluble ATP-binding domain (ATPBD) between TM4 and TM5 (Fig. 1A)[3]. Many P_{1B}-ATPases also include two additional helices preceding TM1. A three amino acid sequence motif in TM4 together with conserved residues in TM5 and TM6 is believed to play a key role in recognizing specific types of metal ions. On the basis of these features and available biochemical data, P_{1B}-ATPases have been classified into seven distinct subfamilies ($_{1B\text{-}1}$ to $_{1B\text{-}7}$)[4]. An additional feature of P_{1B}-ATPases is the presence of soluble metal binding domains (MBDs) at the N- or C-termini. These domains, which are present in the majority of P_{1B}-ATPases, vary in length and composition[4].

Despite the prevalence of these MBDs, most research efforts have focused on one subtype, the prototypical "Atx1-like" domain found in the Cu^+ transporting $P_{1B\text{-}1}$-ATPases. These domains exhibit a βαββαβ fold, similar to that of the copper chaperones in the Atx1 family, and bind Cu^+ via two conserved cysteine residues in a CxxC motif[13,14]. These MBDs can receive Cu^+ from Atx1-like chaperones and also affect the ATPase activity and localization of the $P_{1B\text{-}1}$-ATPases[9]. A similar MBD is found in the Zn^{2+} transporting $P_{1B\text{-}2}$-ATPases[15]. The only other structurally characterized MBD is an unusual cupredoxin-like domain found at the N-terminus of the *Streptococcus pneumoniae* Cu^+ $P_{1B\text{-}1}$-ATPase CopA[16]. A range of histidine-rich N-terminal extensions are present in the Cu^{2+}-transporting $P_{1B\text{-}3}$-ATPases, and one such extension has been demonstrated to affect ATPase activity[17], but none of these putative MBDs have been characterized. Finally, a hemerythrin-like domain that binds a diiron center is present at the C-terminus of many $P_{1B\text{-}5}$-ATPases, but the substrate for this subclass and the role of this domain have not been elucidated[18,19].

A recent bioinformatics analysis suggests that these MBDs may represent just a fraction of those that are present in nature. Within the seven subfamilies, a variety of N- or C-terminal extensions containing potential metal binding residues are present, particularly in the $P_{1B\text{-}2}$, $P_{1B\text{-}3}$, $P_{1B\text{-}4}$, and $P_{1B\text{-}5}$ groups. Interestingly, the majority of these sequences are not predicted to have known folds, suggesting that new types of MBDs may be present[4]. Within the $P_{1B\text{-}4}$ family, which is characterized by six TM helices, conserved SCP (TM4) and HEGT motifs (TM6), and the ability to transport Co^{2+} (Fig. 1A) [19-21], we identified a number of sequences that contain soluble N-terminal extensions with a high percentage of histidine, cysteine, methionine, glutamic acid, and aspartic acid residues. To investigate the possible presence of a new type of MBD, we biochemically, spectroscopically, and structurally characterized the N-terminal MBD from the Cd^{2+}-, Co^{2+}-, and Zn^{2+}-transporting $P_{1B\text{-}4}$-ATPase *Cupriavidus metallidurans* CzcP[22]. The structure reveals a

unique fusion of two ferredoxin-like folds housing two metal binding sites. Activity assays indicate that this domain is necessary for maximal ATPase activity and suggest a role for the MBD in labilizing thiol-bound metal ions. Furthermore, mutations of key residues in either metal binding site have different effects both in vitro and in vivo, suggesting that each may play a unique role in regulating metal transport.

RESULTS

Expansion of the P_{1B-4}-ATPase subfamily

We previously used a combination of Transitivity Clustering and Protein Similarity Networks to reexamine the P_{1B}-ATPases in a systematic manner and identified several new P_{1B-4} sequences with N-terminal extensions[4]. Here we combed the NCBI database to double the number of P_{1B-4} sequences (Supplementary Results, Supplementary Table 1) and generated a new protein similarity network. An examination of protein length (Fig. 1B) and amino acid composition of the N-terminal regions (Fig. 1C) revealed that the majority of the P_{1B-4} subfamily members contain ~150 residue N-terminal extensions rich in potential metal binding residues; some of these extensions also contain CxxC motifs. By constrast, the previously characterized P_{1B-4}-ATPases lack N-terminal extensions[19-21]. While studies of these simpler enzymes established Co^{2+} as a common substrate, our analysis indicated that P_{1B-4}-ATPases with N-terminal extensions were likely more representative of this subfamily on the whole. One P_{1B-4}-ATPase with a putative N-terminal MBD is CzcP from the Gram-negative, metal-tolerant β-proteobacterium *Cupriavidus metallidurans*. Previous work on CzcP indicates that it can transport Cd^{2+}, Co^{2+}, and Zn^{2+} [22]. We hypothesized that the 187 amino acid CzcP N-terminal extension (Figs. 1B, C and Supplementary Fig. 1A) might play a role in mediating differential metal ion selectivity.

Binding of Cd^{2+}, Co^{2+}, and Zn^{2+} by the CzcP MBD

We expressed and purified a protein corresponding to the first 187 amino acids of CzcP (CzcP MBD) and investigated its metal binding properties. We obtained the N-terminally Strep tagged CzcP MBD in high yield and purity (~ 4 mg/L culture, Supplementary Fig. 1B). We then assessed the metal binding properties of the CzcP MBD. When purified in the absence of EDTA, the CzcP MBD contained ~ 0.6 Zn^{2+} (Supplementary Table 2). When we then purified the CzcP MBD in the presence of EDTA, exchanged the MBD into a buffer lacking EDTA, and added 10 mol eq. Cd^{2+} or Co^{2+} to the apo protein, ~ 2 mol eq. of either metal bound to the CzcP MBD, which suggested the presence of two metal binding sites (Supplementary Table 2). When we added 10 mol eq. Zn^{2+} to the apo CzcP MBD, complete precipitation of the protein resulted; 5 mol eq. was the maximum Zn^{2+} that could be added. Similar to the Cd^{2+} and Co^{2+} results, 2 Zn^{2+} bound to the apo CzcP MBD (Supplementary Table 2). These data indicated that the CzcP N-terminal extension is indeed a MBD and that there are two metal binding sites.

Circular dichroism (CD) spectra of the various metal-loaded constructs suggested that only modest changes in secondary structure occur upon metal loading (Fig. 2A). The spectrum of the apo protein was dominated by two local minima in the 200 – 230 nm region, which indicated a mixture of α-helices and β-sheets and thus demonstrated that the MBD was

folded in the absence of metal. Upon metal loading, we observed slight changes in the CD spectra. The spectra of the Cd^{2+}- and Zn^{2+}-loaded MBD differed the most; deconvolution of these spectra suggested an ~ 8-19 % increase in α-helical character and an ~ 6-10 % decrease in β-sheet character compared to the apo MBD spectrum[23,24]. However, this change in secondary structure may be an overestimation since ligand-to-metal charge-transfer (LMCT) transitions of Cys(thiolate) coordinated Cd^{2+}- and Zn^{2+}-bound peptides and proteins (*vide infra*) may be optically active and overlap in the near-UV region[25]. Overall, the Co^{2+}-loaded form exhibited a CD spectrum most similar to that of the apo MBD (Fig. 2A).

The electronic absorption spectrum of the Co^{2+}-loaded CzcP MBD (Fig. 2B) displayed three main features: two strong LMCT transitions at 315 nm and 428 nm ($\varepsilon \sim 7.8\ mM^{-1}\cdot cm^{-1}$ and $\sim 5.1\ mM^{-1}\cdot cm^{-1}$), and a broad d→d absorption feature ($\varepsilon \sim 1.0$ to $0.2\ mM^{-1}\cdot cm^{-1}$) in the 500-700 nm range. The d→d absorption features are consistent with the presence of tetrahedrally coordinated high-spin Co^{2+} [26-28]; the UV LMCT transition is commonly observed for high-spin Cys(thiolate)-ligated Co^{2+} cations[26,27]. The visible LMCT transition is unusual, but may represent a coordinated TCEP molecule (*vide infra*). These data suggested that each of the metal binding sites in the CzcP MBD is tetrahedral and coordinated by at least one Cys(thiolate) ligand, of which two (Cys^{23} and Cys^{54}) exist in the CzcP MBD (Supplementary Figs. 1A,2).

We took advantage of the ability to generate a substoichiometric and a fully Zn^{2+}-loaded form of the CzcP MBD and analyzed both via X-ray absorption spectroscopy (XAS). Simulations of the data for the Zn K-edge extended X-ray absorption fine structure (EXAFS) of the partially (< 1 mol eq.) Zn^{2+}-loaded CzcP MBD (Figs. 2C,D) were best fitted with O/N environments at 1.92 Å and 2.05 Å as the nearest neighbor ligands, as well as an S environment at 2.32 Å (Supplementary Table 3). Long range scattering (> 2.5 Å) was fitted with C environments at 2.97 Å, 3.20 Å, 3.40 Å, and 3.99 Å; C fits at 3.0, 3.2 and 4.0 Å suggested the presence of imidazole scattering around the Zn binding site, which was further confirmed by the signature camelback pattern observed in the EXAFS. These data are consistent with a Zn^{2+} environment consisting of a short Zn^{2+}-O/N bond, likely deriving from a Glu or Asp, a longer Zn^{2+}-O/N bond likely deriving from a His imidazole, and a Zn^{2+}-S bond from a Cys residue. For the fully Zn^{2+}-loaded form of the CzcP MBD, the EXAFS data (Figs. 2E,F) were again fitted with O/N environments, this time at 1.99 Å and 2.12 Å, as well as an S environment at 2.29 Å with long range C scattering at 3.08 Å, 3.29 Å, 3.49 Å, and 4.03 Å (Supplementary Table 3).

Crystal structure of the CzcP MBD

We attempted to crystallize the apo, Cd^{2+}-, Co^{2+}-, and Zn^{2+}-loaded forms of the CzcP MBD. Needle-like crystals of the Cd^{2+}-loaded sample appeared within 1-2 days; the crystals then grew in three dimensions and reached their maximal size (~ 2 mm × 0.5 mm × 0.5 mm) within approximately 1 week. These crystals formed regardless of whether we loaded the CzcP MBD with Cd^{2+} prior to gel filtration chromatography and then attempted crystallization, or if we crystallized the apo CzcP MBD in a drop containing $CdSO_4$. We obtained no crystals for the Co^{2+}- or Zn^{2+}-loaded forms, regardless of how the metal-loaded

protein was generated, and exhaustive trials failed to generate any crystals of the apo domain.

The 2.17 Å resolution (Supplementary Table 4) structure of the Cd^{2+}-loaded CzcP MBD revealed a fusion of the ferredoxin-like motif and the presence of two tetrahedral metal binding sites in a single polypeptide that comprises the asymmetric unit. The overall architecture of the CzcP MBD consists of two distinct domains with a repeating βαββα fold (Figs. 3A,B and Supplementary Figs. 2,3A); this fold is nearly identical to the symmetric ferredoxin-like βαββαβ fold present in the P_{1B-1}- and P_{1B-2}-ATPase MBDs and the Atx1-like copper chaperones[13]. In the CzcP MBD, it appears as if this fold has been duplicated, but the final β strand of the domain 1 has been fused with the ensuing first β strand of domain 2 (β_4: residues 82-88) (Figs. 3A,B). In addition, α_2 from domain 1 is approximately 1.5 turns (six amino acids) longer than the equivalent α helix in other ferredoxin-like P_{1B}-ATPase MBDs. Interestingly, domain 2 has much higher average B factors than domain 1 (Supplementary Fig. 4).

Consistent with the metal binding and spectroscopic data, two Cd^{2+} binding sites, both with His and Cys ligation, are present. The first site (metal binding site 1) is solvent exposed with Cd^{2+} ligated tetrahedrally by His^{41} (β_2), Cys^{54} (β_3), and His^{56} (β_3), all from domain 1, and the phosphine of a TCEP molecule from the buffer. The second Cd^{2+} site (metal binding site 2) is also tetrahedral and is ligated by Asp^{21} and Cys^{23} from domain 1 (α_1) and His^{84} and Glu^{125} from domain 2 (β_4 and β_6, respectively) (Fig. 3 C,D and Supplementary Fig. 5). This site, along with salt bridges between Arg^{81} (α_2, domain 1) and Asp^{127} (β_6, domain 2) and between Asp^{18} (loop between β_1 and α_1, domain 1) and Arg^{123} (β_6, domain 2) (Supplementary Fig. 5), forms the domain-domain interface. The tetrahedral geometry and presence of Cys ligands corroborated the spectroscopic results for the Co^{2+}- and Zn^{2+}-loaded CzcP MBD and implied that the Cd^{2+}-, Co^{2+}-, and Zn^{2+}-binding sites are the same. The presence of Glu and Asp coordination in metal binding site 2 is consistent with the EXAFS data for the partially loaded sample and suggests that this site is of higher affinity and is occupied before metal binding site 1. This observation is consistent with the lack of a fourth protein-derived ligand coordinated to the site 1 Cd^{2+} ion in the crystal structure. It is striking that, despite the similarity in fold, the CzcP MBD does not bind metal ions with a CxxC motif; in fact, very few of the predicted MBDs in the P_{1B-4} subfamily contain CxxC motifs (Fig. 1C). Instead, we found that the metal binding DxC and CxH motifs in the CzcP MBD are conserved in at least 80% of the P_{1B-4}-ATPase N-terminal extensions (Supplementary Fig. 6), which suggested that these metal binding sites may be common. However, the incomplete conservation of these residues implied that not every P_{1B-4}-ATPase N-terminal MBD binds metal in this exact manner, leaving open the possibility that a diversity of MBDs may be present in this subfamily.

We compared the core CzcP MBD βαββα fold with various βαββαβ MBDs and copper chaperones and found that metal binding site 2 is located in the same position as the Atx1-like metal binding CxxC motifs (Supplementary Fig. 7). For example, we superposed the second domain of the Menkes disease protein (ATP7A domain 2) with Cu^+ bound[29] on domain 1 the CzcP MBD, which yielded an rmsd of 0.89 Å for 37 Cα atoms (data not shown). The ATP7A domain 2 Cu^+ coordinating CxxC residues (Cys^{14} and Cys^{17}) occupy

the same position as Cd^{2+} ligands Asp^{21} and Cys^{23} from CzcP MBD domain 1. However, the Cd^{2+} site includes the two additional ligands from domain 2 and is thus buried at the domain interface rather than exposed at the surface. Metal binding site 1 is not present in any other MBD, and its presence leads to a lengthening of strands β_2 and β_3 as well as a short helical turn in the loop connecting these two strands. This distortion, along with the elongation of helix α_2, renders domain 1 less similar to the CxxC-containing MBDs than domain 2; superposition of multiple domains on domain 2, including the MBDs from Ccc2[30], ZntA[15], CadA[31], and domain 6 of the Wilson disease protein[32], yielded rmsd values of ~1 Å (data not shown). However, we found no metal binding site in the CzcP MBD at the position of the CxxC motif in these domains. Instead, the positions corresponding to the two cysteine residues are occupied by His^{94} and Arg^{97}. Thus, the prototypical CxxC-containing βαββαβ fold has evolved into a completely different type of MBD.

Differential occupancy of the two metal binding sites

To investigate whether buried metal binding site 2 is loaded prior to solvent-exposed metal binding site 1 as suggested by the Zn^{2+} EXAFS data, we expressed, purified, and monitored Co^{2+} binding by two variant MBD proteins, D21A/C23A and C54A/H56A, which were designed to selectively disrupt metal binding sites 2 and 1, respectively (Supplementary Fig. 1). For each variant, we monitored the appearance of the Cys(thiolate)-Co^{2+} LMCT at 315 nm (*vide supra*) as a function of added Co^{2+} (Supplementary Fig. 8A,B). While the C54A/H56A variant (site 2 intact) displayed saturating behavior as a function of Co^{2+} concentration with a K_d value of 6.1 ± 4.3 μM, the D21A/C23A variant (site 1 intact) did not saturate over the concentrations of Co^{2+} tested. These data suggested that either site 1 has exceptionally low affinity for Co^{2+} or, alternatively, a slow k_{on} rate, at least in the absence of site 2. A slow k_{on} rate was supported by two observations. First, the electronic absorption spectrum of the D21A/C23A variant incubated overnight with Co^{2+} and desalted displayed the strong LMCT transition at 315 nm consistent with formation of the Cys(thiolate)-Co^{2+} interaction (Supplementary Fig. 8C). Second, overnight incubation of the WT MBD with excess Co^{2+} resulted in binding of 2 mol. eq. of Co^{2+} (*vide supra*), which demonstrated stable binding of Co^{2+} at both metal binding sites. These findings are consistent with the notion that site 2 is occupied prior to site 1 in the isolated, intact MBD.

Effect of the MBD on full length CzcP ATPase activity

To probe the function of the CzcP MBD and its metal binding sites, we expressed, solubilized in dodecyl-β-D-maltopyranoside (DDM), and purified the WT, D21A/C23A, C54A/H56A, and ΔMBD forms of membrane-bound CzcP in high yield and purity (2-6 mg/L culture; Supplementary Fig. 1). The WT construct displayed ATPase activity in a metal-dependent manner, as determined by the malachite green assay (Table 1, Fig. 4A). Its activity was specifically stimulated by the addition of exogenous Cd^{2+}, Co^{2+}, and Zn^{2+}, with maximal ATP hydrolysis in the presence of 50 μM (final concentration) exogenous Cd^{2+} (Fig. 4B; V_{max} = 200 ± 10 nmol $P_i \cdot mg^{-1} \cdot min^{-1}$). Addition of 50 μM Co^{2+} and Zn^{2+} stimulated WT CzcP activity approximately four-fold and five-fold less, respectively; this activity was still significantly higher than that in the presence of other metal ions as well as the basal ATPase activity (Fig. 4A). The K_m values for detergent-solubilized CzcP (Table 1) were similar in magnitude to those reported for vesicle transport assays on this enzyme[22],

but indicated a different order of sensitivity: K_m Zn^{2+} < Cd^{2+} ~ Co^{2+} as compared to Cd^{2+} < Zn^{2+} < Co^{2+} [22]. The lower K_m value for Zn^{2+} suggested that CzcP may be most responsive to fluctuations in environmental Zn^{2+} concentrations, which is consistent with the observed sensitivity of the isolated CzcP MBD to high levels of exogenously added Zn^{2+} ions (*vide supra*).

Mutations of key residues in either metal binding site 1 (C54A/H56A) or metal binding site 2 (D21A/C23A) resulted in enzymes with high basal ATPase rates (Table 1, compare basal activity to WT). That such high rates of ATP hydrolysis occured in the absence of any metal substrate, whereas the WT enzyme required metal substrate to reach similar ATP hydrolysis rates, suggested that metal transport and ATP hydrolysis had become uncoupled in the metal binding site variants. Interestingly, the activity of the C54A/H56A variant was not stimulated by any metal substrate (data not shown), but the D21A/C23A variant displayed weak Cd^{2+}- dependent stimulation with a K_m value of 0.38 ± 0.34 μM as compared to 2.4 ± 0.61 μM for the WT CzcP. Thus, in addition to displaying high basal ATPase activity, the D21A/C23A variant was somewhat more sensitive to exogenous Cd^{2+} than the WT CzcP (Table 1). Neither variant demonstrated Co^{2+}- or Zn^{2+}-stimulated activity (data not shown).

Deletion of the CzcP MBD lowered the maximal rate of ATP hydrolysis and recapitulated the altered sensitivity of the enzyme to exogenous metal observed for the D21A/C23A variant (Table 1). The ΔMBD CzcP displayed the same activity trend (V_{max} ΔMBD CzcP +Cd^{2+} > +Co^{2+} > +Zn^{2+}) as the WT, but the Cd^{2+}- and Zn^{2+}-stimulated activities were reduced by ~ 40% whereas the Co^{2+}-stimulated activity was decreased by ~ 10%. This behavior was different from that of the metal binding site variants and suggested that the complete absence of the MBD alleviated any enzymatic uncoupling. One potential explanation for this observation is that the MBD interacts directly with the ATPBD or AD. In the metal binding site variant proteins, the MBD and ATPBD and/or AD may be locked in an unproductive conformation that stimulates ATP hydrolysis, but blocks the metal entryway. In this scenario, complete removal of the MBD might not only alleviate the unproductive conformation, but also provide access to the TM region that might be otherwise inaccessible in the metal binding site variants. However, any differential sensitivity towards metal substrate might be affected by removing the MBD. Consistent with this hypothesis and similar to the D21A/C23A variant, deletion of the MBD increased the sensitivity of the enzyme towards Cd^{2+} and Co^{2+}, which resulted in K_m values for these substrates comparable to that of the Zn^{2+}-stimulated enzyme (Table 1), and further suggested that the MBD is responsible for regulation in this enzyme.

We also measured metal-dependent activity in the presence of various thiols, including glutathione, *L*-cysteine, and DTT. Cysteine is required for maximal activity of the P_{1B-1}-ATPase CopA from *Archaeoglobus fulgidus*[33] and the P_{1B-2}-ATPase ZntA from *E. coli*[34]. Here, thiols primarily decreased or did not affect WT CzcP activity (Supplementary Fig. 9A). However, we observed moderate increases in activity upon addition of Zn^{2+} with DTT (~ 25%) or Co^{2+} with GSH (~ 20%) (Supplementary Fig. 9A). Assayed under identical conditions, the ΔMBD CzcP did not display these moderate increases in activity (Supplementary Fig. 9B), which suggested that the presence of the MBD aids in labilization of these thiophilic metals under certain conditions, perhaps due to competitive chelation.

Metal resistance enhancement in *E. coli*

To assess the physiological role of the CzcP MBD and its metal binding sites, we transformed our *E. coli* expression strain with the various full length CzcP constructs and monitored growth on agar plates supplemented with different concentrations of $CdSO_4$ and IPTG. Since *E. coli* has its own Zn- and Cd-transporting P_{1B-2}-ATPases, we hypothesized that expression of CzcP would enhance Cd^{2+} resistance, as it does in *C. metallidurans* and metal-sensitive strains of *E. coli*[22]. Growth of *E. coli* bearing either the empty plasmid or WT CzcP was completely abrogated at Cd^{2+} concentrations > 1.0 mM and an IPTG concentration of 0.1 mM (data not shown) whereas growth appeared normal in the absence of $CdSO_4$. Western blotting analysis demonstrated that WT CzcP is expressed under these conditions (Supplementary Fig. 10A). After 24 h incubation at 37°C in the presence of 0.1 mM IPTG, spot assays indicated a dense ring of bacterial growth for cells bearing all expression plasmids. When 1.0 mM $CdSO_4$ was included, colonies were only observed for the *E. coli* expressing WT CzcP (Supplementary Fig. 10B). After 48 h incubation at 37°C, it was clear that the *E. coli* expressing WT CzcP had a distinct growth advantage on $CdSO_4$-supplemented agar plates compared to *E. coli* with the empty plasmid (Fig. 4C). Thus, our *E. coli* expression strain appeared to utilize CzcP as a resistance enhancer, as has been previously shown for a metal-sensitive strain[22].

Using this system, we then investigated the effects of CzcP variant expression on Cd^{2+} sensitivity. The CzcP variants were clearly expressed in the presence of 0.1 mM IPTG but the absence of Cd^{2+} (Supplementary Fig. 10A). Consistent with our hypothesis that metal transport may be hindered in the metal binding site variants, we observed minimal growth for the D21A/C23A or C54A/H56A variants on 1.0 mM $CdSO_4$-supplemented plates after 24 h and 48 h incubation at 37°C (Supplementary Fig. 10B and Fig. 4C, respectively). However, in the presence of 0.75 mM $CdSO_4$, bacterial growth and protein expression were evident after 24 h for both the WT and the D21A/C23A variant, but there was minimal growth for either the empty plasmid or the C54A/H56A variant (Supplementary Fig. 10B). After 48 h incubation, it was clear that the C54A/H56A variant mirrored the minimal growth pattern of the empty plasmid (Fig. 4C). Deletion of the MBD in its entirety affected growth similarly to expression of the D21A/C23A variant. After 24 h at 37°C, expression of the ΔMBD CzcP appeared to be capable of conferring Cd^{2+} resistance, albeit at a lower Cd^{2+} concentration than WT CzcP despite similar levels of protein expression (Supplementary Figs. 10A,B). In contrast to the C54A/H56A variant, the ΔMBD variant enhanced resistance to 0.75 mM $CdSO_4$ (Supplementary Fig. 10), but like the D21A/C23A variant, growth of *E. coli* expressing the ΔMBD variant was strongly diminished on 1.0 mM $CdSO_4$ even after 48 h incubation (Fig. 4C).

DISCUSSION

A previously undetected type of P_{1B}-ATPase MBD has been identified and characterized for the P_{1B-4}-ATPase subfamily. The observed stimulation of CzcP ATPase activity in the presence of Cd^{2+}, Co^{2+}, or Zn^{2+} combined with the binding of all three metal ions to its N-terminal MBD are consistent with prior results indicating that CzcP mediates Co^{2+} resistance and functions in concert with P_{1B-2}-ATPases to enhance Cd^{2+} and Zn^{2+}

resistance[22]. Hitherto unseen in any P_{1B}-ATPase, the CzcP MBD includes ferredoxin-like folds resembling those in Atx1-like MBDs and chaperones, but fused in a unprecedented two-domain arrangement that houses two unique metal binding sites. Removal of this MBD reduced ATPase activity significantly, consistent with the MBD playing a positive allosteric regulatory role, as has been suggested for MBDs from the CopA-like P_{1B-1}-ATPases[35,36] as well as the C-terminal MBD of the *Arabidopsis thaliana* HMA2 P_{1B-2}-ATPase[37]. In contrast, deletion of the proposed Zn^{2+}/Cd^{2+} chelating C-terminus from the P_{1B-2}-ATPase *Arabidopsis thaliana* HMA4 upregulates the P_{1B}-ATPase, suggesting an autoinhibitory role for this domain[38].

We propose that the two metal binding sites play distinct roles in mediating metal transport. Metal binding site 1, which is solvent accessible, could be responsible for acquiring metal and may act as a potential metallochaperone, delivering metal to the TM region. The presence of an exogenous TCEP ligand indicates that ligand exchange can occur at this site, and the modest effects of DTT and GSH on activity suggests a role for the MBD in mediating exchange with thiol ligands, possibly by competitive chelation. It is notable that CzcP lies outside of the main *czc* operon on the *C. metallidurans* pMOL30 plasmid[39]. The nearest gene for a possible stand-alone metallochaperone within the vicinity of the *czcP* gene is *czcE*, which encodes a periplasmic copper-binding protein and is unlikely to target CzcP given its metal substrates[40,41]. Thus, in contrast to CopA systems that have cognate Atx1-like[13] or CupA[16] chaperones, metal binding site 1 may function as an internal metallochaperone, acquiring metal from small ligands or polypeptides, and possibly mediating direct delivery to the TM region. The observed slow or low affinity binding of Co^{2+} to this site may suggest that transient or weak interactions with metal occur at this site, or that a ligand from the TM region entryway is also involved in binding. Although no structural information exists to indicate which metal binding site may be part of the metal transfer pathway, removal of the highly conserved CxH motif in metal binding site 1 appeared to uncouple ATPase activity from metal transport and prevented enhanced Cd^{2+} resistance for *E. coli* cells expressing this variant. We envision that this uncoupling may result from the inability of metal binding site 1 to deliver metal to the TM region or from blocking entry of metal into the TM region. Complete removal of the MBD appeared to abrogate this enzymatic uncoupling as it restored ATP hydrolysis in response to metal concentration, and it appeared to confer a Cd^{2+} resistance enhancement in *E. coli*. However, in the absence of the MBD, the maximal rate of ATP hydrolysis in vitro was lowered compared to WT, and there appeared to be a lower level of resistance enhancement in vivo.

Metal binding site 2, which is located at the domain interface, may function as a metal sensor. In this hypothetical scenario, domain 2 is flexible in the absence of metal, but metal binding locks it in place with domain 1, which could alter interactions of the MBD with the ATPBD, AD, or TM region, similar to a proposed function for the C-terminal *Arabidopsis thaliana* HMA2 MBD[37]. Consistent with this notion, domain 2 displays much higher average B factors (Supplementary Fig. 4) than domain 1, and 40 residues at the C-terminus of domain 2 (residues 167-208) were not visible in the electron density map. Furthermore, the inability to crystallize the apo form despite exhaustive trials suggests a high level of conformational flexibility in the absence of metal. Interestingly, removal of the DxC motif

in metal binding site 2 sensitized both the isolated variant CzcP enzyme and *E. coli* expressing this variant to exogenous Cd^{2+}. These observations were mirrored upon removal of the MBD both in vitro and in vivo, strongly suggesting that the MBD DxC motif regulates function. EXAFS data for the partially and fully Zn^{2+}-loaded MBD and Co^{2+}-binding studies indicated that metal binding site 2 is occupied before metal binding site 1, which would be consistent with this site controlling metal transport prior to metal delivery to the TM region. Conformational changes upon metal binding to site 2 could be transmitted to domain 1 via two loop regions adjacent to the CxH and DxC motifs (Supplementary Fig. 4). These loop regions are more extended than the corresponding loops in MBDs from other P_{1B}-ATPases (Supplementary Fig. 7), and may be instrumental in coupling metal binding at the proposed sensory site to metal delivery to the proposed chaperone site. Investigation of this model, which represents a new mechanism of P_{1B}-ATPase regulation, is underway.

ONLINE METHODS

Materials

Buffers, salts and glycerol were purchased from Sigma-Aldrich, RPI, or VWR and used as received, unless otherwise noted.

Protein similarity network generation

The protein similarity network of the P_{1B-4}-ATPases was generated as described previously[4] with an input of 200 protein sequences (Supplementary Table 1). Protein similarity networks and sequence attributes were generated in Cytoscape (v. 2.8.3) and visualized using the VizMapper plug-in.

Cloning and expression of CzcP constructs

Wildtype (WT, residues 1-829) and ΔMBD (residues 183-829) CzcP constructs were commercially synthesized by GENEWIZ, Inc. (South Plainfeld, NJ). Briefly, DNA sequences were derived from the gene encoding for CzcP from *Cupriavidus metallidurans* (EMBL identifier ABF12829), with an additionally engineered DNA sequence (5'-GCC-GGC-GAA-AAC-CTG-TAT-TTT-CAG-AGC-GCA-GGC-3') encoding for a C-terminal TEV-protease cleavage site (AGENLYFQSAG). DNA sequences were codon-optimized for expression in *E. coli*, and synthesized genes were subcloned into the pET-21a(+) expression plasmid (EMD Millipore) using the NdeI and XhoI restriction sites, such that the insert was read in-frame with the DNA sequence encoding for the plasmid-derived C-terminal His_6 tag. The CzcP N-terminal MBD (residues 1-182) gene sequence was PCR amplified with PFU Turbo DNA polymerase (Thermo Scientific) using *C. metallidurans* CH34 template genomic DNA (ATCC) and the following primers (Integrated DNA Technologies): forward, 5'-TAC-TTC-CAA-TCC-AAT-GCA-ACC-GAA-AAG-CTG-CGC-CTG-GAC-3'; reverse, 5'-TTA-TCC-ACT-TCC-AAT-GTT-ATT-AGC-CAA-ACA-CGC-TGC-CGT-GTG-C-3'. Primers were designed with specific overhangs (underlined) for ligase-independent subcloning (LIC) into the pBAD Strep TEV LIC cloning vector 8R (plasmid 37506, AddGene), which adds an N-terminal Streptactin-binding sequence (MASWSHPQFEK) and a following N-terminal TEV-protease cleavage site (GAENLYFQSNA). The expression plasmid was linearized with SspI (New England Biolabs), gel purified, and treated with

excess dGTP and LIC-quality T4 DNA polymerase (Thermo Scientific). The PCR product was gel purified and then treated with excess dCTP and LIC-quality T4 DNA polymerase. Vector and insert (2:1, v:v) were incubated at 22°C for 5 min, after which 1 μL of 25 mM EDTA solution was added, and the resulting mixture was incubated for another 5 min at 22°C. This mixture (2 μL) was then transformed into E. cloni 10G chemically competent cells (Lucigen), spread onto Luria-Bertani (LB) agar plates supplemented with 100 μg/mL ampicillin and grown overnight at 37°C. The correctly inserted gene product was verified by sequencing of the grown individual colonies (ACGT, Inc.). The D21A/C23A and C54A/H56A MBD variants were commercially synthesized by GENEWIZ, Inc. (South Plainfeld, NJ). Mutations D21A/C23A and C54A/H56A of the membrane-bound CzcP were introduced using the QuikChange Lightning Multi Site-Directed Mutagenesis Kit (Agilent). Plasmid DNA of the WT CzcP in the pET-21a(+) expression vector served as the template for mutagenesis, and the following primers were used to introduce the mutated bases (underlined): 5'-GCAGACGCTCAACGGCAGGGGCGCTACTATCCGGC-3' and 5'-GCCGGATAGTAGCGCCCCTGCCGTTGAGCGTCTGC-3' (D21A/C23A); 5'-CTAATGGCTGCCGGATCATAAGCCACGGCAATCTGACTATCGCTATCCAC-3' and 5'-GTGGATAGCGATAGTCAGATTGCCGTGGCTTATGATCCGGCAGCCATTAG-3' (C54A/H56A). The presence of each mutation was verified by automated DNA sequencing (ACGT Inc.).

Expression of WT, ΔMBD, D21A/C23A, and C54A/H56A CzcP constructs was performed in a similar manner. Chemically competent BL21 (DE3) *E. coli* cells (Millipore) were transformed with the appropriate plasmid and grown overnight in sterilized LB media supplemented with 100 μg/mL ampicillin. Overnight cultures were used to inoculate baffled flasks containing 1 L of sterilized LB media supplemented with 100 μg/mL ampicillin. Cells were grown at 37°C with shaking at 160 rpm until the OD_{600} reached a value of ~ 0.6-0.8. Protein expression was induced by the addition of 1 mL of 1 M isopropyl β-D-1-thiogalactopyranoside (IPTG), at which point the temperature was lowered to 18°C and shaking was continued at 160 rpm. Cells were harvested ~ 18 hr later by spinning at 4800 × *g* for 10 min in a Sorvall SLC 4000 rotor at 4°C. Cells were resuspended in 25 mM Tris buffer (pH 7.5), 100 mM sucrose, 10 mM EDTA, flash-frozen in $N_{2(l)}$, and stored at −80°C. For the expression of the CzcP MBD, chemically competent Top10 *E. coli* cells (Life Technologies) were transformed with the appropriate plasmid and grown overnight in sterilized LB media supplemented with 100 μg/mL ampicillin. Overnight cultures were used to inoculate unbaffled flasks containing 1 L of sterilized LB media supplemented with 100 μg/mL ampicillin. Cells were grown at 37°C with shaking at 160 rpm until the OD_{600} reached a value of ~ 0.6-0.8. Protein expression was induced by the addition of 1 mL of 20% (w/v) L-(+)-arabinose, at which point the temperature was lowered to 30°C and shaking was continued at 160 rpm. Cells were harvested ~ 4 hr later by centrifuging at 4800 × *g* for 10 min in a Sorvall SLC 4000 rotor at 4°C. Cells were resuspended in 50 mM Tris buffer (pH 7.5), 20 mM NaCl, 5% (v/v) glycerol, flash-frozen in $N_{2(l)}$, and stored at −80°C.

Purification of CzcP constructs

All steps during the purification procedure were carried out at 4°C unless otherwise noted. Cells containing the expressed WT and ΔMBD CzcP constructs were thawed and

homogenized via stirring. Solid phenylmethylsulfonyl fluoride (PMSF, Pierce; 50-100 mg) and solid deoxyribonuclease I (Bovine, Sigma-Aldrich; 50-100 mg) were both added immediately prior to lysing the cell solution by multiple passes through a 15,000 psi microfluidizer cooled with a slurry of ice, water, and 70% (v/v) EtOH. Cellular debris was pelleted via centrifugation at 8000 × *g* for 45 min. The remaining supernatant was decanted and membranes were pelleted by ultracentrifugation at 163,000 × *g* for 1 hr. Membranes were then washed and homogenized in fresh resuspension buffer (25 mM Tris buffer (pH 7.5), 100 mM sucrose, 10 mM EDTA with 50-100 mg PMSF added prior to homogenization) before being pelleted again by ultracentrifugation at 163,000 × *g* for 45 min. Washed and pelleted membranes were resuspended in resuspension buffer in which the EDTA had been omitted. The concentration of protein in these membranes was determined using the detergent-compatible Lowry (DC) assay (Bio-Rad). Protein was solubilized by the addition of a 10% (w/v) stock *n*-dodecyl-β-D-maltopyranoside (DDM) to ~ 1% (w/v) final detergent concentration and ~ 3 mg/mL final protein concentration with vigorous stirring for ~ 2 hr. The solution was clarified by ultracentrifuging at 163,000 × *g* for 45 min. The supernatant was then applied to two tandem 5 mL HiTrap Chelating HP columns (GE Healthcare) that had been charged with Ni^{2+} and equilibrated with 8 column volumes (CVs) of buffer A (25 mM Tris (pH 8.0), 100 mM sucrose, 500 mM NaCl, 0.05% (w/v) DDM) with an additional 21 mM imidazole. The column was then washed with 12 CVs of buffer A with an additional 50 mM imidazole. Both constructs were then eluted by washing with buffer A containing an additional 150 mM imidazole. Fractions were concentrated using a 15 mL Amicon 100 kDa MWCO spin concentrator (Millipore) and buffer exchanged by repeated concentration and dilution steps in the same spin concentrator into 25 mM Tris (pH 8.0), 100 mM sucrose, 50 mM NaCl, 1 mM TCEP, 0.02% (w/v) DDM. Protein concentration was determined using the DC Lowry assay, and purity was assessed via 15% SDS-PAGE analysis.

Purification of the CzcP MBD was initiated as described above; once thawed and homogenized, cells were lysed via sonication for a total of 12 min using 15 s on pulses and 30 s rest pulses. All insoluble material was pelleted by ultracentrifugation at 163,000 × *g* for 1 h, and the resulting supernatant was applied to a 20-mL streptactin column (Qiagen) equilibrated with 50 mM Tris (pH 7.5), 200 mM NaCl, 10% (v/v) glycerol. After extensive washing, bound protein was eluted with buffer containing 50 mM Tris (pH 7.5), 200 mM NaCl, 2.5 mM D-desthiobiotin, 10% glycerol and ± 10 mM EDTA, depending on the experimental conditions. Fractions were concentrated using a 15 mL Amicon 10 kDa MWCO spin concentrator and applied to a 120 mL Superdex 75 (GE Healthcare) gel filtration column that had been preequilibrated with 25 mM Tris (pH 7.5), 100 mM NaCl, 1 mM TCEP, 2.5% (v/v) glycerol. The eluted fractions corresponding to the protein monomer (~ 23 kDa) were pooled and concentrated using another 15 mL Amicon 10 kDa MWCO spin concentrator. Protein concentration was determined using the DC Lowry assay.

ATPase activity assays

The rate of ATP hydrolysis was determined using the malachite green assay[42]. Briefly, stocks of WT and ΔMBD CzcP were diluted to 0.05-0.10 mg/mL using stock buffer with a final composition of 100 mM Tris (pH 7.5), 3 mM $MgCl_2$, 100 mM NaCl, 10 mM TCEP,

0.1 mg/mL asolectin, and 0.01% (w/v) DDM. For metal stimulation assays, stock solutions of the metal salt ($MnCl_2$, $FeC_6H_5O_7$, $NH_4Fe(SO_4)_2$, $CoCl_2$, $NiCl_2$, $CuCl_2$, $ZnCl_2$, $CdSO_4$, or $Pb(CH_3COO)_2$) were added to a final concentration of 50 μM except when assaying the specific activity vs. $[M^{2+}]$, in which metal concentration varied from 0.5-100 μM. For Cu^+ assays, TCEP was omitted and replaced by 1 mM DTT. Thiol competition assays were performed under the same conditions as the native assay except the assay buffer contained an additional 10 mM reduced DTT, reduced *L*-Cys, or reduced glutathione (GSH). Assays containing Cu^+ and Fe^{2+} were conducted under an inert atmosphere in a Coy glovebox (Coy Laboratory Products, Inc.). Stock solutions of substrate (Na_2ATP, 1.5 mM final concentration) were added to initiate the reaction; assays were carried out in 1.5 mL eppendorf tubes at 30°C with 300 rpm shaking for 10-15 min, depending on the construct. The reaction was then immediately halted by addition of a 3:1 (v:v) ratio of working solution (1.05% (w/v) ammonium molybdate tetrahydrate, 0.0338% (w/v) malachite green carbinol, 1.0 M HCl) to protein assay solution. After addition of 100 μL 34% (w/v) sodium citrate, the absorbance at 660 nm of the enzyme-containing solution was measured using an Agilent 8453 spectrophotometer, and $[P_i]$ was interpolated using a standard curve. Specific activity data are corrected against background hydrolysis of Na_2ATP in the absence of enzyme ± metal cations.

Plated assays

The effect of recombinant expression of CzcP and its variants on the growth of *E. coli* BL21(DE3) (Millipore) was assessed visually by monitoring the growth of cells on LB agar plates with and without $CdSO_4$ and/or IPTG. Briefly, *E. coli* BL21(DE3) was transformed with either the empty pET-21a(+) expression plasmid (EMD Millipore) or one of the following constructs: WT, ΔMBD, D21A/C23A, or C54A/H56A CzcP. Single colonies of cells bearing one of these plasmids were grown in 100 mL LB broth supplemented with 100 μg/mL ampicillin overnight by shaking at 200 rpm at 37°C. The optical density (OD_{600}) was measured, and the cells were diluted to an OD_{600} = 0.06 in fresh, sterile LB broth. 5 μL of this solution were plated in triplicate onto LB agar plates supplemented with 100 μg/mL ampicillin and various combinations of ± 0.050 mM IPTG, 0.10 mM IPTG, 0.75 mM $CdSO_4$, 1.0 mM $CdSO_4$, and/or 10 mM $CdSO_4$. These plates were incubated at 37°C, and cell growth was assessed after 24, 48, and 60 h. Each plate experiment was repeated in duplicate. Protein expression was assessed by growing *E. coli* BL21(DE3) containing either the empty expression plasmid or one of the CzcP construct expression plasmids in liquid culture under conditions similar to the plated assays. Cells were harvested and membranes isolated as described (*vide supra*). Membranes were resolubilized in 10% (w/v) SDS, and total membrane protein was quantified using the DC Lowry assay. For cells grown in the absence of Cd^{2+}, 4 μg of total membrane protein were run on 15% SDS-PAGE. Because cell growth was greatly diminished in the presence of Cd^{2+}, only a maximum of 1 μg of total membrane protein was run on 15% SDS-PAGE under this condition. Protein expression was confirmed by Western blotting followed by immunostaining with an anti $(His)_6$ antibody (Sigma Aldrich).

Metal loading and analysis

Metal-loading analyses were performed on the CzcP MBD in the final exchange buffer (*vide supra*) with an additional 400 mM NaCl and 20% (v/v) glycerol. Loading of Cd^{2+} and Co^{2+} was achieved via slow addition of 10 mol. eq. of the buffered metal cation solution at 4°C to the apo protein that had been purified in the presence of EDTA. Addition of Zn^{2+} to the apo protein solution that had been purified in the presence of EDTA caused almost complete precipitation after addition of ~ 5 mol. eq. so no more than this amount was added. In all cases, after complete addition of any metal cation to the CzcP MBD, the solution was rocked gently overnight (typically 12-16 hr) at 4°C. Excess metal was removed via several repeated concentration and dilution steps with fresh buffer in a 0.5 mL Amicon spin concentrator (10 kDa MWCO). Final protein concentrations were determined using the DC Lowry assay. For metal analysis, protein was digested in ~ 5 mL 3% TraceSelect HNO_3 (Sigma Aldrich), and any aggregated protein was pelleted via centrifugation at 5000 × *g* for 10 min. Standards containing Cd^{2+}, Co^{2+}, and Zn^{2+} were similarly prepared in 3% TraceSelect HNO_3. Metal content was measured using a Varian Vista MPX inductively-coupled plasma optical-emission spectrometer (ICP-OES; Integrated Molecular Structure Education and Research Center, Northwestern University). Data were interpolated from linear curves generated using standard solutions of known concentration and are the average of three independent samples deriving from at least two independent protein preparations.

Electronic absorption and circular dichroism spectroscopies

All electronic absorption spectra were collected at room temperature using an Agilent 8453 UV-Vis spectrophotometer set to a spectral bandwidth of 1 nm. Protein was contained in a 1 cm pathlength quartz cuvette. Circular dichroism (CD) spectra were collected at 20°C using a Jasco J-815 spectropolarimeter set to a spectral bandwidth of 1 nm. Protein was contained in a 0.6 mm quartz cuvette, and spectra are the average of 5 cumulative scans. CD spectra were deconvoluted using the DichroWeb online server (http://dichroweb.cryst.bbk.ac.uk/html/home.shtml)[23,24]. Metal-binding curves were performed in a similar manner as the metal-loading for ICP-OES analysis (*vide supra*) with the following modifications: 20% (v/v) glycerol was exchanged for 2.5% (v/v) and equilibration was performed at 20°C. Mixtures of protein and metal were allowed to equilibrate 5 min at 20°C before the absorbance at 315 nm was monitored and corrected against a reference wavelength of 900 nm. Each metal binding experiment was performed in triplicate on the same protein preparation. Binding isotherms for the C54A/H56A variant were fitted in Igor Pro v. 6.04 (WaveMetrics, Inc.). Dissociation constants represent the average of three independent trials on the same protein preparation ± one standard deviation of the mean.

X-ray absorption spectroscopy

Samples of the CzcP MBD partially (< 1 mol eq.) and fully (2 mol eq.) reconstituted with Zn^{2+} were resuspended in 25 mM Tris HCl (pH 7.5), 100 mM NaCl, 10 mM TCEP and 30% glycerol, and loaded into Lucite cells wrapped with Kapton tape, flash frozen in liquid nitrogen and stored at −80°C until data collection. Zn XAS data were collected at the National Synchrotron Light Source on beamlines X3A and X3B. Beamline X3A was equipped with a sagittally focusing Si[220] double crystal monochromator followed by a

downstream cylindrically bent palladium-coated harmonic rejection mirror, while beamline X3B was equipped with a sagittally focusing Si[111] double crystal monochromator with a downstream cylindrically bent nickel-coated harmonic rejection mirror. During data collection, samples were maintained at 25 K on beamline X3A and at 14K on beamline X3B, both using He Displex cryostats. Zinc fluorescence excitation spectra were collected using a 13-element Canberra Ge solid-state detector on beamline X3A and using a 31-element Canberra Ge fluorescence detector on beamline X3B. Copper filters (3 to 6 μm) were placed between the cryostat and detector to filter background scattering fluorescence not associated with protein Zn signals while collecting Zn data. XAS spectra were measured in 5 eV steps in the pre-edge region (9350-9640 eV), 0.25 eV steps in the edge region (9640-9690 eV), and 0.05 $Å^{-1}$ increments in the EXAFS region (to k = 13 $Å^{-1}$ for Zn), integrating from 1s to 14s in a k^3 weighted manner for a total scan length of approximately 45 min. X-ray energies were internally calibrated collecting Zn foil absorption spectra simultaneously with protein data. The monochromator was calibrated for each spectrum based on the first inflection point of the Zn foil spectrum (assigned to 9659 eV).

Spectral analysis was accomplished using established protocols[43]. Each fluorescence channel of each scan was examined for spectral anomalies prior to averaging. The represented data are the average of ten to twelve scans. XAS data were processed using the Macintosh OS X version of the EXAFSPAK program suite (wwwssrl.slac.stanford.edu/~george/exafspak/exafs.htm) integrated with the Feff v. 8 software[44] for theoretical model generation. Data reduction utilized a polynomial function in the pre-edge region and a three-region cubic spline throughout the EXAFS region. Data were converted to k-space using an E_0 value of 9680 eV for Zn. The k-cubed weighted EXAFS was truncated at 1.0 and 12.88 $Å^{-1}$ for Zn filtering purposes. These k ranges correspond to spectral resolution of ca. 0.13 Å for all metal-ligand interactions under consideration; therefore only independent scattering environments outside 0.13 Å were considered resolvable in the EXAFS fitting analysis[45]. Zn EXAFS fitting analysis was performed on raw/unfiltered data also using single scattering Feff theoretical models calculated for oxygen, sulfur, and carbon coordination to simulate the nearest neighbor ligand environments. During data simulation, a scale factor of 1.0 and threshold energy of −15.25 eV was utilized for Zn-O/N/C and S scattering. Scale factors and E_0 values used during the simulations were calibrated by fitting crystallographically characterized models in different metal oxidation states, as described previously[46]. Criteria for judging the best-fit simulation utilized both the lowest mean square deviation between data and fit corrected for the number of degrees of freedom (F')[43], and a reasonable Debye-Waller factor ($\sigma^2 < 0.006$ $Å^2$).

Crystallization, data analysis, and structure determination

Crystals of the Cd^{2+}-loaded CzcP MBD were obtained by the sitting-drop vapor-diffusion method using MiTeGen-XtalQuest Plates with a 1:1 (v:v) apo protein (10 mg/mL) and reservoir solution mixture at room temperature. The preciptant solution consisted of 0.1 M MES (pH 6.0) 15% (w/v) PEG 4000, 1 mM $CdSO_4$. Long three-dimensional, colorless needles appeared within 24 hr and reached their maximal size within 1 week. Crystals were transferred into a cryoprotectant that consisted of the precipitant solution plus 25% (v/v) glycerol; after soaking 1 min, crystals were looped, flash-frozen in $N_{2(l)}$ and stored at 77 K.

Data sets were collected on beamlines LS-CAT 21-ID-D and GM/CA-CAT 23-ID-D at the Advanced Photon Source, Argonne National Laboratory, using Mar 300 CCD and Pilatus3 6M detectors, respectively. Data were processed automatically with Xia2[47], and phases and initial models were generated using the AutoSol and AutoBuild programs in Phenix[48]. Extended model building and refinement cycles were performed in Coot[49] and REFMAC5[50,51], respectively. Restraints for Cd^{2+}-ligand bonds were generated automatically in REFMAC5; descriptions of the TCEP molecule were generated with the program JLigand[52] utilizing the appropriate library obtained from the Grade Web Server (http://grade.globalphasing.org/cgibin/grade/server.cgi). A final restrained refinement was performed using these combined libraries in REFMAC5, and final validations were performed using Phenix Validate and the CheckMyMetal web server (http://csgid.org/csgid/metal_sites/). The final model consists of residues 21-167; the remaining 40 residues were not observed in the electron density map. Data collection and refinement statistics are presented in Supplemtary Table 4. Ramachandran statistics indicate that 97% of residues fall in the allowed region, 3% of residues fall in the generously allowed region, and 0% of residues fall in the disallowed region. Structural overlays and Cα RMSD values were generated and calculated by utilizing UCSF Chimera (v. 1.6).

Accession codes

The atomic coordinates for the CzcP MBD have been deposited in the Protein Data Bank, Research Collaboratory for Structural Bioinformatics at Rutgers University (deposition ID: 4U9R).

Statistical analysis of data

Statistical analysis of crystallographic data was performed automatically in all respective software (*vide supra*) and is presented without modification. Statistical analysis of XAS data was performed automatically in the EXAFSPAK program suite (*vide supra*) and is presented without modification. All other statistical analyses were performed within the Igor Pro v. 6.04 software. Reported values represent the average of three independent trials and are given ± one standard deviation of the mean unless otherwise noted. Curve fitting in Igor Pro was accomplished using a non-linear least squares fit, and fitted values were derived from this analysis.

Supplementary Material

Refer to Web version on PubMed Central for supplementary material.

Acknowledgements

This work was supported by National Institutes of Health Grants GM58518 (A. C. R.), DK068139 (T. L. S.), F32GM105339 (A. T. S.), and T32HL120822 (D. B.). Sequence searches utilized both database and analysis functions of the Universal Protein Resource (UniProt) Knowledgebase and Reference Clusters (http://www.uniprot.org) and the National Center for Biotechnology Information (http://www.ncbi.nlm.nih.gov/). Portions of this research were carried out at the National Synchrotron Light Source (NSLS). NSLS, located at Brookhaven National Laboratory, is supported by the U.S. Department of Energy, Division of Materials Sciences and Division of Chemical Sciences, under Contract No. DE-AC02-98CH10886.

Abbreviations

AD	actuator domain
ATP	adenosine-5’-triphosphate
ATPBD	ATP-binding domain
CD	circular dichroism
DDM	dodecyl-β-D-maltopyranoside
DTT	dithiothreitol
EDTA	ethylenediaminetetraacetic acid
EXAFS	extended X-ray absorption fine structure
GSH	reduced glutathione
***L*-Cys**	*L*-Cysteine
MBD	metal-binding domain
RMSD	root-mean-square deviation
TCEP	*tris*(2-carboxyethyl)phosphine
TM	transmembrane helix
WT	wildtype
XAS	X-ray absorption spectroscopy

References

1. Palmgren MG, Nissen P. P-Type ATPases. Ann. Rev. Biophys. 2011; 40:243–266. [PubMed: 21351879]
2. Argüello JM. Identification of ion-selectivity determinants in heavy-metal transport P_{1B}-type ATPases. J. Membr. Biochem. 2003; 195:93–108.
3. Argüello JM, Eren E, González-Guerrero M. The structure and function of heavy metal transport P_{1B}-type ATPases. Biometals. 2007; 20:233–248. [PubMed: 17219055]
4. Smith AT, Smith KP, Rosenzweig AC. Diversity of the metal-transporting P_{1B}-type ATPases. J. Biol. Inorg. Chem. 2014; 19:947–960. [PubMed: 24729073]
5. Argüello JM, González-Guerrero M, Raimunda D. Bacterial transition metal P_{1B}-ATPases: transport mechanism and roles in virulence. Biochemistry. 2011; 50:9940–9949. [PubMed: 21999638]
6. Rosenzweig, AC.; Arguello, JM. Toward a molecular understanding of metal transport by $P1_B$-type ATPases.. In: Lutsenko, S.; Argüello, JM., editors. Metal Transporters. Vol. 69. Elsevier Academic Press Inc; San Diego: 2012. p. 113-136.
7. Williams LE, Mills RF. P_{1B}-ATPases - an ancient family of transition metal pumps with diverse functions in plants. Trends Plant Sci. 2005; 10:491–502. [PubMed: 16154798]
8. Gupta A, Lutsenko S. Evolution of copper transporting ATPases in eukaryotic organisms. Current Genom. 2012; 13:124–133.
9. Lutsenko S, Gupta A, Burkhead JL, Zuzel V. Cellular multitasking: The dual role of human Cu-ATPases in cofactor delivery and intracellular copper balance. Arch. Biochem. Biophys. 2008; 476:22–32. [PubMed: 18534184]
10. Andersson M, et al. Copper-transporting P-type ATPases use a unique ion-release pathway. Nature Struct. Molec. Biol. 2014; 21:43–48. [PubMed: 24317491]

11. Gourdon P, et al. Crystal structure of a copper-transporting PIB-type ATPase. Nature. 2011; 475:59–74. [PubMed: 21716286]
12. Wang K, et al. Structure and mechanism of Zn^{2+}-transporting ATPase. Nature. 2014; 514:518–522. [PubMed: 25132545]
13. Boal AK, Rosenzweig AC. Structural biology of copper trafficking. Chem. Rev. 2009; 109:4760–4779. [PubMed: 19824702]
14. Singleton C, LeBrun NE. Atx1-like chaperones and their cognate P-type ATPases: copper-binding and transfer. Biometals. 2007; 20:275–289. [PubMed: 17225061]
15. Banci L, et al. A new zinc-protein coordination site in intracellular metal trafficking: solution structure of the apo and Zn(II) forms of ZntA(46-118). J. Mol. Biol. 2002; 323:883–897. [PubMed: 12417201]
16. Fu Y, et al. A new structural paradigm in copper resistance in *Streptococcus pneumoniae*. Nature Chem. Biol. 2013; 9:177–183. [PubMed: 23354287]
17. Mana-Capelli S, Mandal AK, Argüello JM. *Archaeoglobus fulgidus* CopB is a thermophilic Cu^{2+}-ATPase. J. Biol. Chem. 2003; 278:40534–40541. [PubMed: 12876283]
18. Traverso ME, et al. Identification of a hemerythrin-like domain in a P_{1B}-type transport ATPase. Biochemistry. 2010; 49:7060–7068. [PubMed: 20672819]
19. Zielazinski EA, Cutsail GE III, Hoffman BM, Stemmler TL, Rosenzweig AC. Characterization of a cobalt-specific P_{1B}-ATPase. Biochemistry. 2012; 51:7891–7900. [PubMed: 22971227]
20. Raimunda D, Long JE, Sassetti CM, Arguello JM. Role in metal homeostasis of CtpD, a Co2+ transporting P_{1B4}-ATPase of *Mycobacterium smegmatis*. Mol. Microbiol. 2012; 84:1139–1149. [PubMed: 22591178]
21. Raimunda D, Long JE, Padilla-Benavides T, Sassetti CM, Arguello JM. Differential roles for the Co^{2+}/Ni^{2+} transporting ATPases, CtpD and CtpJ, in *Mycobacterium tuberculosis* virulence. Mol. Microbiol. 2014; 91:185–197. [PubMed: 24255990]
22. Scherer J, Nies DH. CzcP is a novel efflux system contributing to transition metal resistance in *Cupriavidus metallidurans* CH34. Molec. Microbiol. 2009; 73:601–621. [PubMed: 19602147]
23. Whitmore L, Wallace BA. DICHROWEB, an online server for protein secondary structure analyses from circular dichroism spectroscopic data. Nucl. Acids Res. 2004; 32:W668–W673. [PubMed: 15215473]
24. Whitmore L, Wallace BA. Protein secondary structure analyses from circular dichroism spectroscopy: Methods and reference databases. Biopolymers. 2008; 89:392–400. [PubMed: 17896349]
25. Zelazowski AJ, Szymanska JA, Law AYC, Stillman MJ. Spectroscopic Properties of the α Fragment of Metallothionein. J. Biol. Chem. 1984; 259:12960–12963. [PubMed: 6386806]
26. Frankel AD, Berg JM, Pabo CO. Metal-dependent folding of a single zinc finger from transcription factor IIIA. Proc. Natl. Acad. Sci. USA. 1987; 84:4841–4845. [PubMed: 3474629]
27. Giedroc DP, Keating KM, Martin CT, Williams KR, Coleman JE. Zinc metalloproteins involved in replication and transcription. J. Inorg. Biochem. 1986; 28:155–169. [PubMed: 3543219]
28. Maret W, Vallee BL. Cobalt as probe and label of proteins. Methods Enzymol. 1993; 226:52–71. [PubMed: 8277880]
29. DeSilva TM, Veglia G, Opella SJ. Solution structures of the reduced and Cu(I) bound forms of the first metal binding sequence of ATP7A associated with Menkes disease. Proteins. 2005; 61:1038–1049. [PubMed: 16211579]
30. Banci L, Bertini I, Ciofi-Baffoni S, Huffman DL, O'Halloran TV. Solution structure of the yeast copper transporter domain Ccc2a in the apo and Cu(I) loaded states. J. Biol. Chem. 2001; 276:8415–8426. [PubMed: 11083871]
31. Banci L, et al. Structural basis for metal binding specificity: the N-terminal cadmium binding domain of the P1-type ATPase CadA. J. Mol. Biol. 2006; 356:638–650. [PubMed: 16388822]
32. Achila D, et al. Structure of human Wilson protein domains 5 and 6 and their interplay with domain 4 and the copper chaperone HAH1 in copper uptake. Proc. Natl. Acad. Sci. USA. 2006; 103:5729–5734. [PubMed: 16571664]

33. Mandal AK, Cheung WD, Argüello JM. Characterization of a thermophilic P-type Ag^{+}/Cu^{+}-ATPase from the extremophile *Archaeglobus fulgidus*. J. Biol. Chem. 2002; 277:7201–7208. [PubMed: 11756450]
34. Sharma R, Rensing C, Rosen BP, Mitra B. The ATP hydrolytic activity of purified ZntA, a Pb(II)/Cd(II)/Zn(II)-translocating ATPase from Escherichia coli. J. Biol. Chem. 2000; 275:3873–3878. [PubMed: 10660539]
35. Mandal AK, Argüello JM. Functional roles of metal binding domains of the *Archaeoglobus fulgidus* Cu^{+}-ATPase CopA. Biochemistry. 2003; 42:11040–11047. [PubMed: 12974640]
36. Mattle D, et al. On allosteric modulation of P-Type Cu^{+}-ATPases. J. Mol. Biol. 2013; 425:2299–2308. [PubMed: 23500486]
37. Eren E, Kennedy DC, Maroney MJ, Argüello JM. A novel regulatory metal binding domain is present in the C terminus of *Arabidopsis* Zn2+-ATPase HMA2. J. Biol. Chem. 2006; 281:33881–33891. [PubMed: 16973620]
38. Bækgaard L, et al. A combined zinc/cadmium sensor and zinc/cadmium export regulator in a heavy metal pump. J. Biol. Chem. 2010; 285:31243–31252. [PubMed: 20650903]
39. Monchy S, et al. Plasmids pMOL28 and pMOL30 of *Cupriavidus metallidurans* Are Specialized in the Maximal Viable Response to Heavy Metals. J. Bacteriol. 2007; 189:7417–7425. [PubMed: 17675385]
40. Zoropogui A, Gambarelli S, Covés J. CzcE from *Cupriavidus metallidurans* CH34 is a copper-binding protein. Biochem. Biophys. Res. Commun. 2008; 365:735–739. [PubMed: 18029263]
41. Petit-Haertlein I, et al. Evidence for conformational changes upon copper binding to *Cupriavidus metallidurans* CzcE. Biochemistry. 2010; 49:1913–1922. [PubMed: 20112954]
42. Lanzetta PA, Alvarez LJ, Reinach PS, Candia OA. Improved assay for nanomole amounts of inorganic-phosphate. Anal. Biochem. 1979; 100:95–97. [PubMed: 161695]
43. Bencze, KZ.; Kondapalli, KC.; Stemmler, TL. X-ray absorption spectroscopy.. In: Scott, RA.; Lukehart, CM., editors. Applications of Physical Methods to Inorganic and Bioinorganic Chemistry: Handbook, Encyclopedia of Inorganic Chemistry. John Wile & Sons, Ltd; Chicester, UK: 2007. p. 513-528.
44. Ankudinov AL, Rehr JJ. Relativistic calculations of spin-dependent X-ray absorption spectra. Phys. Rev. B. 1997; 56:R1712–R1715.
45. Lee PA, Citrin PH, Eisenberger P, Kincaid BM. Extended X-ray absorption fine structure - its strengths and limitations as a structural tool. Rev. Mod. Phys. 1981; 53:769–806.
46. Wang B, et al. Structure and ubiquitin interactions of the conserved zinc finger domain of Np14. J. Biol. Chem. 2003; 278:20225–20234. [PubMed: 12644454]
47. Winter G. *xia2*: an expert system for macromolecular crystallography data reduction. J. Appl. Cryst. 2010; 43:186–190.
48. Adams PD, et al. PHENIX: a comprehensive Python-based system for macromolecular structure solution. Acta Cryst. 2010; D66:213–221.
49. Emsley P, Cowtan K. Coot: model-building tools for molecular graphics. Acta Cryst. 2004; D60:2126–2132.
50. Winn MD, et al. Overview of the CCP4 suite and current developments. Acta Cryst. 2011; D67:235–242.
51. Murshudov GN, et al. REFMAC5 for the refinement of macromolecular crystal structures. Acta Cryst. 2011; D67:355–367.
52. Lebedev AA, et al. JLigand: a graphical tool for the CCP4 template-restraint library. Acta Cryst. 2012; D68:431–440.

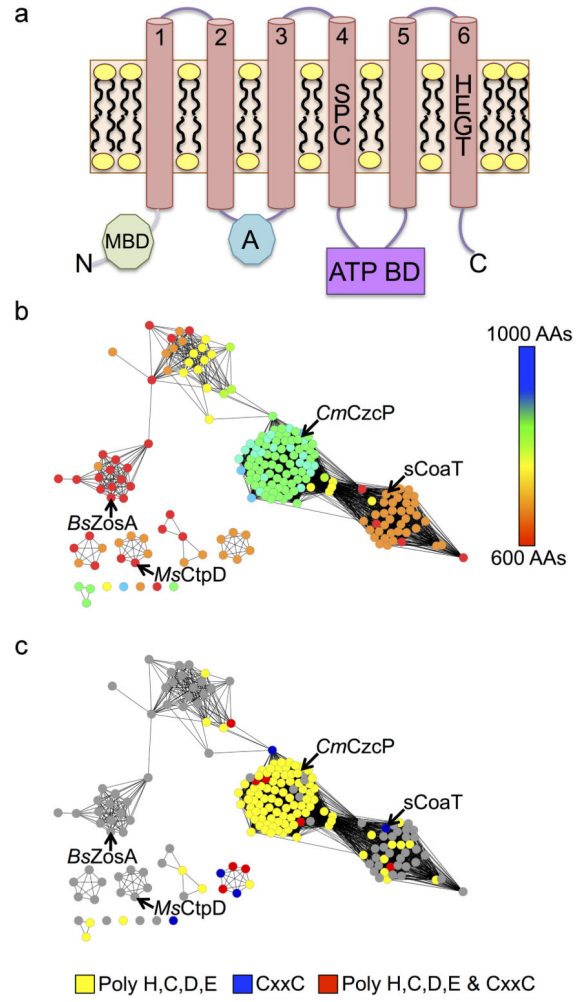

Figure 1. The P_{1B-4}-ATPase subfamily

(**a**) Overall topology of a P_{1B-4}-ATPase in a membrane, including the six transmembrane helices (cylinders), the metal binding domain (MBD; green polygon), the actuator domain (A; blue polygon), and the ATP binding domain (ATP BD; purple rectangle). (**b**) and (**c**) The P_{1B-4}-ATPase protein similarity network color-coded on the basis of polypeptide length and rough composition of the N-terminal extension. In panel (**b**), the approximate number of amino acids (AAs) is indicated based on the colored scale to the right. In panel (**c**), the presence of His, Cys, Asp, and Glu residues (H,C,D,E) and/or the presence of a CxxC motif are indicated. The previously studied P_{1B-4}-ATPases are labeled in both panels: *Cupriavidus metallidurans* CzcP (*Cm*CzcP), *Bacillus subtilis* ZosA (*Bs*ZosA), *Sulfitobacter sp*. NAS-14.1 (sCoaT), and *Mycobacterium smegmatis* CtpD (*Ms*CtpD).

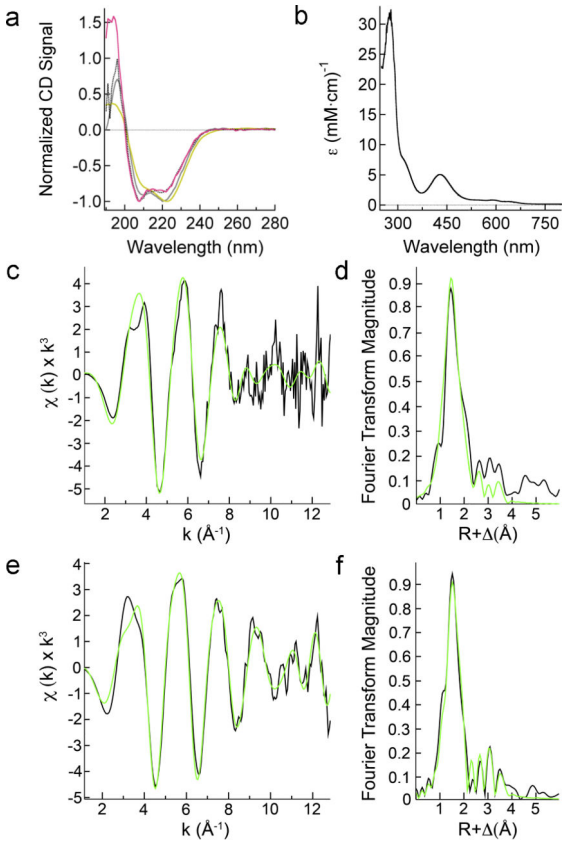

Figure 2. Spectroscopic characterization of the *C. metallidurans* CzcP metal binding domain (MBD)

(**a**) Circular dichroism spectra of the apo (dashed), Cd^{2+}- (yellow), Co^{2+}- (pink), and Zn^{2+}-loaded (gray) CzcP MBD. (**b**) Electronic absorption spectrum of the Co^{2+}-loaded CzcP MBD plotted as molar absorptivity (ε, $mM^{-1}\cdot cm^{-1}$) vs. wavelength (nm). (**c**,**d**) The raw (black) and simulated (green) k^3-weighted EXAFS data (**c**) and phase-shifted Fourier transforms (**d**) of the partially Zn^{2+}-loaded CzcP MBD. (**e**,**f**) The raw (black) and simulated (green) k^3-weighted EXAFS data (**e**) and phase-shifted Fourier transforms (**f**) of the fully Zn^{2+}-loaded CzcP MBD. Fitted data indicate a mixture of N-, O-, and S-containing nearest-neighbor ligands to the Zn^{2+} ions (Supplementary Table 3).

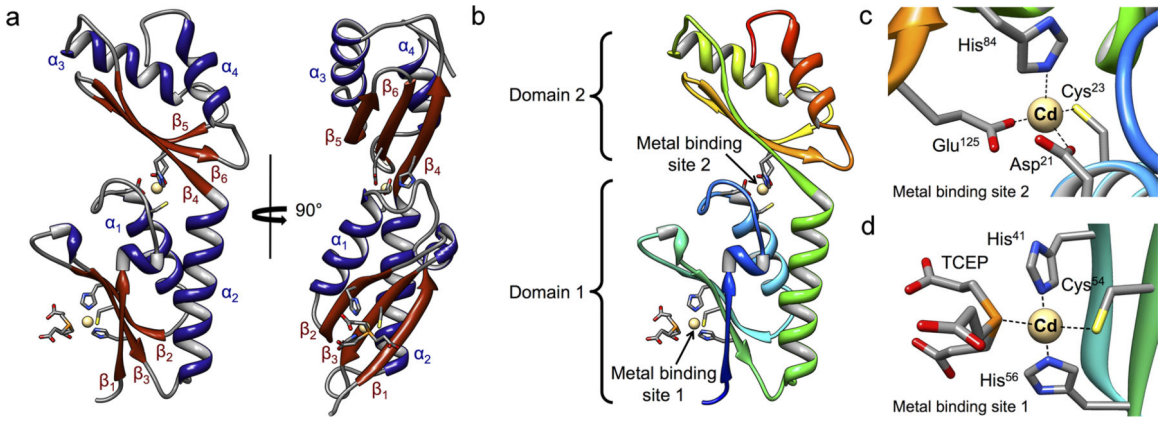

Figure 3. The *C. metallidurans* CzcP metal binding domain (MBD)

(**a**) The crystal structure of the CzcP MBD (corresponding to residues 2-145 from the intact WT CzcP P_{1B-4}-ATPase) colored with α helices in blue and β sheets in red, both of which are numbered sequentially. (**b**) The domain arrangement and metal binding sites in the CzcP MBD. The CzcP MBD is rainbow colored from N-terminus (blue) to C-terminus (red) with locations of domains and metal binding sites labeled. (**c**) Close-up view of the domain-domain interface metal binding site. (**d**) Close-up view of the solvent-exposed metal binding site.

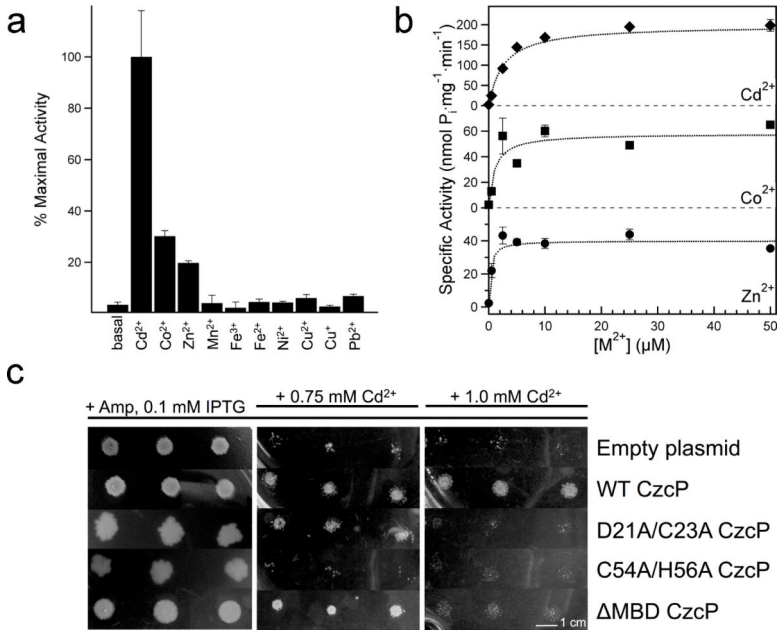

Figure 4. Functional characterization of CzcP

(**a**) Percent maximal ATP hydrolysis activity of detergent-solubilized CzcP in the presence of 50 μM (final concentration) M^{n+}. The graph is shown relative to 100% activity, which is defined as the highest observable activity under identical conditions tested (50 μM Cd^{2+}, 200 ± 10 nmol $P_i \cdot mg^{-1} \cdot min^{-1}$). Error bars represent ± one standard deviation of the average of at least three independent experiments on the same protein preparation. (**b**) Specific activity vs. $[M^{2+}]$ graphs in the presence of varying concentrations of Cd^{2+} (diamonds), Co^{2+} (squares), and Zn^{2+} (circles). Error bars represent ± one standard deviation of the average of at least three independent experiments on the same protein preparation. Curves were fitted to the equation $y = (V_{max} \cdot x) / (K_m + x)$ in Igor Pro v. 6.04. (**c**) Plated assays of *E. coli* BL21(DE3) growth demonstrating the effects of expression of WT and variant CzcP constructs on Cd^{2+} resistance. Pictures of spot assays show *E. coli* growth at 37°C on LB agar plates supplemented with 100 μg/mL ampicillin after 24 h growth on plates also supplemented with 0.1 mM IPTG (left panel), 48 h growth on plates also supplemented with 0.1 mM IPTG and 0.75 mM Cd^{2+} (middle panel), and 48 h growth on plates also supplemented with 0.1 mM IPTG and 1.0 mM Cd^{2+} (right panel). Cells were plated in triplicate, and each plate was grown under identical conditions in duplicate. The white line in the lower right corner represents a 1 cm scale bar.

Table 1

Kinetic parameters of detergent-solubilized CzcP ATP hydrolysis activity.

CzcP Construct	Metal Added (50 μM)	Basal Activity (nmol $P_i \cdot mg^{-1} \cdot min^{-1}$)	V_{max} (nmol $P_i \cdot mg^{-1} \cdot min^{-1}$)	K_m (μM)
WT	—	2.4 ± 0.83	—	—
	Cd^{2+}		200 ± 10	2.4 ± 0.61
	Co^{2+}		58 ± 5.8	1.0 ± 0.64
	Zn^{2+}		40 ± 2.4	0.29 ± 0.16
D21A/C23A	—	130 ± 29	—	—
	Cd^{2+}		166 ± 19	0.38 ± 0.34
C54A/H56A	—	180 ± 40	—	—
ΔMBD	—	13 ± 6.2	—	—
	Cd^{2+}		120 ± 3.5	0.42 ± 0.10
	Co^{2+}		56 ± 4.0	0.10 ± 0.12
	Zn^{2}+		22 ± 2.8	0.36 ± 0.41

Data values are reported as the average ± one standard deviation of at least three experiments on the same protein preparation.